Lane Change–Intention Inference and Trajectory Prediction of Surrounding Vehicles on Highways

Jongyong Do, Kyoungseok Han, *Member, IEEE,* and Seibum B. Choi, *Member, IEEE*

***Abstract*—The behavior prediction of the surrounding vehicles is crucial when planning a minimal-risk path when realizing a collision-avoidance system. Herein, we propose a multiple model–based adaptive estimator (MMAE) that infers the lane-change intention of the surrounding vehicles and then predicts their trajectories. Specifically, first, a path is generated in the form of a cubic spline curve using the Frenet coordinate system, which is robust to changes in road curvatures. Linearized recursive least-squares estimation (LRLSE) method is used to adaptively predict a future trajectory based on the past trajectory of the target vehicle. Preview time is defined as a time-varying parameter that determines the final point of the path, and LRLSE updates it in real time. The MMAE applies LRLSEs to multiple paths and obtains the mode probability for each path, then the lane-change intention is inferred using the mode probability and preview time. The predicted future trajectory is the cubic spline curve determined based on the preview time. Further, we verify the performance of our approach using highD, a naturalistic dataset of vehicle trajectories, and compare it with those of existing methods. The proposed method does not require a large amount of data for training and has a low computational burden and high real-time performance.**

***Index Terms*—Lane-change intention, linearized recursive least-squares estimation, multiple model–based adaptive estimator, trajectory prediction**

I. INTRODUCTION

A. Motivation and Related Research

ADVANCED driver assistance systems (ADAS) have been extensively studied with the purpose of enhancing driving safety and comfort. One crucial component of ADAS is the collision avoidance system (CAS), which has been identified as significant in mitigating traffic accidents caused by human error [1]. CAS can be classified into three stages: risk recognition, path planning based on optimal decision-making, and path tracking control [2]. As technology for perceiving the driving environment becomes more reliable, active research is being conducted on decision-making algorithms that aim to minimize the risk of collisions. In particular, lane-change situations, which have the potential to result in fatal outcomes compared to other normal driving scenarios, are receiving close attention [3].

In order to effectively make lane-change decisions for autonomous vehicles (AVs), it is necessary to take into account a comprehensive set of information including the dynamic states and road information. To address this requirement, various learning-based approaches have been proposed. [4] used deep reinforcement learning to realize lane-change decision-making in dynamic and uncertain traffic scenarios. The performance of the algorithm using deep Q-N-network [5] was verified with a real world–like simulator. [6] applied Nash equilibrium and Stackelberg game theory to approach human-like decision-making by considering different driving styles and social interaction characteristics. There is also Nash Q-learning, which is a combination of deep reinforcement learning and game theory, and has only been verified for simple scenarios [7]. In addition, there are methods using support vector machine (SVM) [8] and fuzzy logic [9], but the accuracy is less than 90%, which is not at the level of actual application.

In an ideal case where all vehicles are autonomous vehicles (AVs) and are connected, the lane-change timing of each vehicle can be clearly known and an optimal decision can be made in a given situation [10]. However, generally, not all vehicles can be connected AVs, and human-driven vehicles and nonconnected AVs are mixed. Therefore, lane-change decision-making is highly dependent on the surrounding of an AV. Particularly, AVs can safely change lanes by accurately determining the lane-change intentions of surrounding vehicles.

There are various learning-based methods for lane-change detection of surrounding vehicles, and many studies verify their performance using a dataset such as next-generation simulation (NGSIM). Lane-change predictor using random forest showed high performance with a small window size of 3 s and a $\sim$98.6% accuracy [11]. A long short-term memory (LSTM) neural networks (NN)-based behavior predictor was devised [12]. A hidden Markov model (HMM)-based intention recognizer robust to complex real urban traffic has an accuracy of approximately $\sim$88% and the average recognition time before the lane-change maneuver was 7.08 s for highway datasets [13]. Lane-change intention is determined through

This study was partly supported by the BK21 FOUR Program of the National Research Foundation Korea (NRF) grant funded by the Ministry of Education, Autonomous Driving Technology Development Innovation Program (20018181; Development of Lv. 4+ Autonomous Driving Vehicle Platform based on Point-to-point Driving to Logistic Center for Heavy Trucks) funded by the Ministry of Trade, Industry Energy(MOTIE, Korea) and Korea Evaluation Institute of Industrial Technology(KEIT), the National Research Foundation of Korea (NRF) grant funded by the Korean government (MSIP) (No. 2020R1A2B5B01001531), the Technology Innovation Program (20014983; Development of Autonomous Chassis Platform for a Modular Vehicle) funded by the Ministry of Trade, Industry & Energy(MOTIE, Korea), and the NRF funded by the Korean government, Ministry of Science and ICT (MSIT) under grant NRF-2021R1C1C1003464.

Jongyong Do and Seibum B. Choi (Corresponding author) are with the Korea Advanced Institute of Science and Technology, 291, Daehak-ro Yuseong-gu, Daejeon, 34141, South Korea (e-mails: djy0129@kaist.ac.kr and sbchoi@kaist.ac.kr).

Kyoungseok Han (Cocorresponding author) is with the School of Mechanical Engineering, Kyungpook National University, Daegu 41566, South Korea (e-mail: kyoungsh@knu.ac.kr).

Manuscript received February 26, 2023; revised March 22, 2023.

trajectory prediction of the target vehicle with an average of 1.74 s in advance before the actual lane change [14]. Methods applying SVM and an artificial NN (ANN) recorded accuracies of $\sim$97.1% and $\sim$98.8% respectively [15], but the yaw rate and lateral accelerations used as learning features are difficult to determine unless a V2V environment is present.

The performance of the algorithm was also verified using data acquired through a driving simulator. [16] proposed a lane-change Bayesian network (LCBN) incorporated with a Gaussian mixture model (GMM) (LCBN–GMM). 32 drivers participated in data acquisition. To effectively label data, they proposed a gaze-based labeling (GBL) method by monitoring a driver's gaze behavior. The LCBN–GMM with GBL estimated a driver's lane-change intention, which is an average of 4.5 s ahead of the actual lane-change (with $\sim$78.2% accuracy), considering driving style and contextual traffic. [17] proposed a fuzzy C-means clustering algorithm and an adaptive NN to categorize the dataset and optimize it through the NN.

[18] set the lane-change feasibility and corresponding vehicle trajectory obtained using fuzzy rules as the LSTM input, and this verification was performed using a hardware-in-the-loop system (HILS). There is a study that verified on-road performance through vehicle experiments and drastically reduced the false-positive rate [19]. The back-propagation NN model was verified via vehicle-driving experiments involving 16 experienced drivers and predicted intention 1.5 seconds ahead on average [20].

If the future trajectory is predicted after successfully inferring the lane-change intention of the surrounding vehicles, then the CAS performance becomes more robust. Meanwhile, existing studies on trajectory prediction have progressed from model-based filtering to NN-based learning.

Interactive multiple model trajectory prediction (IMMTP) is a combination of physics- and maneuver-based prediction models, and vehicle experiments verified that IMMTP performs better than a single model [21]. In [22], maneuver classification was performed with SVM, and the final point of the trajectory was determined with quantile regression forests. There is also a method to train Gaussian process models using real-world trajectories of lane-change vehicles, but intention inference of lane-change behavior was not considered [23].

Various studies on trajectory prediction of the surrounding vehicles have used LSTM. A multihead attention–based LSTM (MHA-LSTM) was introduced in [24] and compared with various methods. In [25], after inferring the current maneuver of a preceding target vehicle with LSTM, lane-crossing points are predicted with a model trained with deep NN (DNN) to obtain a future trajectory. [26] applied a deep ensemble technique to a motion prediction model based on LSTM, considering the uncertainty-aware potential field. [27] recognized lane-change intention using SVM-recursive feature elimination in a V2V environment and predicted the trajectory with LSTM. The performance of the model should be improved considering the noise effect and driver characteristics of V2V. In [28], the trajectory was predicted using LSTM, but the states of the surrounding vehicles were not considered. Moreover, [29] and [30] used LSTM to predict future trajectories; however, the consistent performance could not be guaranteed. Another way is to apply Mamdani fuzzy logic [31].

Previous research has employed machine learning (ML) strategies, optimizing performance through careful consideration of various situational factors, leading to generally favorable outcomes. But it requires big data for model training and there is a possibility of overfitting [32]. The complexity of the model, characterized by an increased number of features, may lead to limitations in real-time performance. Recently, ML-based solutions that can operate in real time are coming out because of their good computation efficiency [33].

This study aims to infer the lane-change intention of the surrounding vehicles and predict their future trajectory. Linearized recursive least-squares estimation (LRLSE) is proposed to adapt the cubic spline curve generated in the Frenet coordinate system in real time using the previous trajectory of a target vehicle. To apply each LRLSE to multiple paths, we design a multiple model–based adaptive estimator (MMAE) and then calculate the mode probability for each path. The followings are the main contributions of this study:

(1) We propose LRLSE as a real-time adaptation method of the preview time that determines the final point of a nonlinear cubic spline curve.

(2) If the target vehicle can follow multiple paths, then LRLSE can be used in parallel and an MMAE can be constructed to obtain each mode probability. Each model constituting the MMAE changes according to the driving trajectory of the target vehicle.

(3) The lane-change intention of the target vehicle is inferred from the mode probability and preview time for each path calculated in the MMAE, and subsequently the lane-change trajectory is predicted. The performance of the MMAE is verified using highD, a naturalistic dataset of vehicle trajectories.

B. Paper Organization

The remainder of this paper is organized as follows. Section II discusses coordinate transformation and path generation using the cubic spline curve. Section III presents the preview time adaptation and MMAE design using LRLSE. The performance of the proposed MMAE is verified in Section IV. Finally, Section V provides the conclusion and future work.

II. Coordinate Transformation and Path Generation

In this study, the global (Cartesian) coordinates (x, y) of a lane are assumed to be known using a map. To avoid the influence of road curvature, the global coordinate system is converted to the Frenet coordinate system and the paths that can be followed by the target vehicle are modeled as cubic spline curves [34].

A. Frenet Coordinate System

If the global coordinates of a lane are known, then the coordinates to be followed by the target vehicle can be predicted when maintaining or changing lanes from the current location. Specifically, the coordinates that are expected to be followed by the target vehicle can be expressed as a function

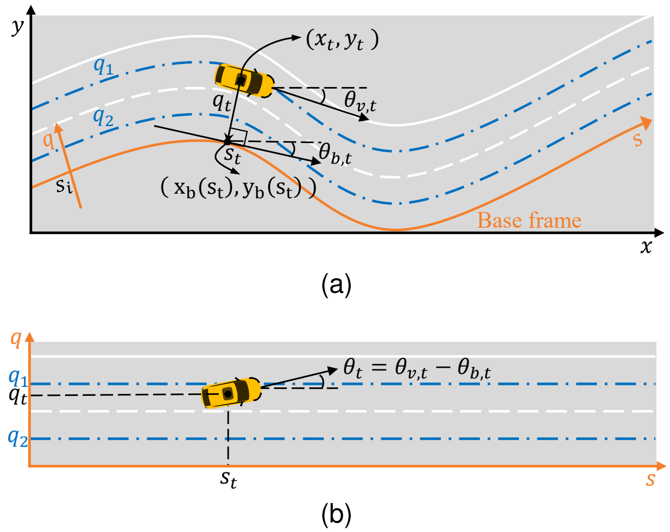

Fig. 1. Coordinate transformation. (a) Global coordinate system and base frame. (b) Frenet coordinate system.

of the global coordinate system. However, if this process is conducted using a global coordinate system, the shape of the function does not appear consistently depending on road curvature. If the road is straight (without any curvature), a path can be generated in a consistent form using the current location of the target vehicle. Therefore, curved roads should be transformed into straight roads to ensure methodological generality, and this curvilinear coordinate system is called a Frenet coordinate system. Figs. 1(a) and 1(b) show the transformation process from the global to the Frenet coordinate system.

Fig. 1(a) presents a curved road in the global x–y coordinate system, and the current location of the target vehicle is at (x_t, y_t). Because the global coordinates of the lanes are known, the position of the target vehicle is indicated with respect to one of the lanes. The standard lane is the base frame, the length of this lane is s, and the vertical distance away from the base frame is q. From the viewpoint regarding vehicle, s and q are the longitudinal travel distance and lateral distance from the base frame, respectively. The base frame is represented by parameterizing x and y in the global coordinate system as the cubic functions for s in ((1) and (2)):

$$x_b(s) = a_{x,i}(s - s_i)^3 + b_{x,i}(s - s_i)^2 + c_{x,i}(s - s_i) + d_{x,i}, \tag{1}$$

$$y_b(s) = a_{y,i}(s - s_i)^3 + b_{y,i}(s - s_i)^2 + c_{y,i}(s - s_i) + d_{y,i}, \tag{2}$$

where $a_{x,i}, b_{x,i}, c_{x,i}$, and $d_{x,i}$ are the coefficients of the cubic spline curve of x with respect to s and $a_{y,i}, b_{y,i}, c_{y,i}$, and $d_{y,i}$ are the coefficients of the cubic spline curve of y with respect to s. When the coordinates x_b and y_b of the base frame are expressed as the parametric curve for s, the sections of the base frame are divided by the s range and the coefficients for each section are obtained. Here, s_i is the s value at the initial position of the i^{th} section.

The section is divided to accurately express a point on the base frame as a spline curve for s. If the points on the long base frame are expressed as a single spline curve, then the error between the actual points and the curve increases. However, if the section is subdivided many times, the amount of calculation is increased. Hence, the length of the section must be appropriately adjusted, and the length of the section can be changed depending on the curvature. In Fig. 1(a), $\theta_{v,t}$ and $\theta_{b,t}$ for the current position of the target vehicle represent the heading angle and the instantaneous inclination in the base frame in the global coordinate system, respectively ((3a) and (3b)).

$$\tan\theta_v = \frac{V_y}{V_x}, \tag{3a}$$

$$\tan\theta_b = \frac{dy}{ds} \cdot \frac{ds}{dx}. \tag{3b}$$

The x and y coordinates of the target vehicle and the velocities V_x and V_y along the x and y directions in the global coordinate system can be measured using a sensor in the ego AV [35] or can be known through V2V communication [36]. Subsequently, s can be obtained using the x and y coordinates, and the slope of the base frame with respect to this s can be obtained. The distance from the base frame to the target vehicle is numerically calculated using Newton's method [37]. The situation in the global coordinate system presented in Fig. 1(a) can be expressed in the Frenet coordinate system (Fig. 1(b)). In the Frenet coordinate system, the current position of the target vehicle is indicated by s_t and q_t and the heading angle is θ_t. Further, θ presents the difference between the heading angle of the vehicle and the angle with respect to the instantaneous inclination in the base frame, as expressed in (4).

$$\theta = \theta_v - \theta_b. \tag{4}$$

B. Path Generation

After transforming a curved road in the global coordinate system into a straight road in the Frenet coordinate system, the paths that can be followed by the target vehicle are modeled in this subsection. In Fig. 2, we assume a three-lane road. Hence, the vehicle is assumed to perform three maneuvers: (i) changing lanes to the left-hand side, (ii) driving in the current lane, and (iii) changing lanes to the right-hand side. The paths for each maneuver can be modeled as a cubic spline curve. The current position of the target vehicle is (s_t, q_t), and the heading angle is θ. q_1, q_2, and q_3 are the q values of each lane center. The path can be expressed as follows:

$$q(s) = a(s - s_t)^3 + b(s - s_t)^2 + c(s - s_t) + d, \quad (s_t \le s \le s_f) \tag{5}$$

where a, b, c, and d are the coefficients of the cubic spline curve (5), which can be determined using four boundary conditions for the initial and final points of the path, as expressed in (6).

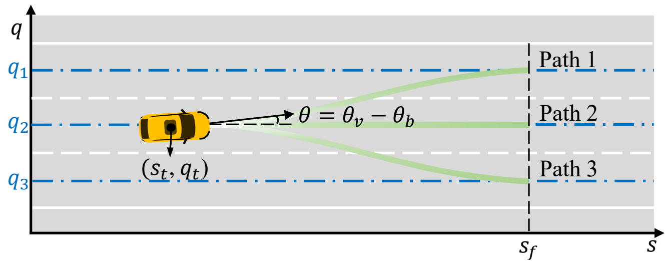

Fig. 2. Path models in the form of cubic spline curves in the Frenet coordinates.

$$
\begin{array}{llll}
1) & q(s_t) = q_t & 2) & \dfrac{dq}{ds}(s_t) = \tan\theta_v - \theta_b \\
3) & q(s_f) = q_i & 4) & \dfrac{dq}{ds}(s_f) = 0.
\end{array} \tag{6}
$$

Conditions 1)–4) relate to the initial coordinates, initial heading angle, final coordinates, and final heading angle of the path, respectively. q_i is the distance from each lane center to the base frame, which is a condition for the final point of the path. For example, as shown in Fig. 2, when the vehicle changes lanes in the direction of increasing q, the q coordinate of the final point is q_1. The s coordinate of the final point, s_f, is set according to the speed of the vehicle and can be expressed as follows:

$$
s_f = V_t t_{prev} + s_t, \tag{7}
$$

where V_t denotes the longitudinal speed, t_{prev} represents the preview time and indicates the time consumed to change a lane, and $s_f - s_t$ denotes the longitudinal distance traveled until the lane change is completed. The result of calculating the coefficients of the cubic spline curve by applying the boundary conditions is expressed as follows:

$$
\begin{aligned}
&\begin{bmatrix} a \\ b \end{bmatrix} = \\
&\begin{bmatrix} (s_f - s_t)^3 & (s_f - s_t)^2 \\ 3(s_f - s_t)^2 & 2(s_f - s_t) \end{bmatrix}^{-1} \begin{bmatrix} q_i - q_t - c(s_f - s_t) \\ -c \end{bmatrix} \\
&c = tan(\theta_v - \theta_b), \quad d = q_t.
\end{aligned} \tag{8}
$$

III. Lane Change–Intention Inference and Trajectory Prediction

A. Preview Time Adaptation via LRLSE

The final point of the path is expressed as in (7), and t_{prev} is the unknown varying parameter, which varies depending on the driver's disposition or the surrounding environment. To express path coefficients a and b with respect to t_{prev}, (7) is substituted into (5) and the boundary conditions for the final point are applied. Coefficients c and d are determined by the initial coordinates and heading angle.

$$
a = \frac{V_t c t_{prev} + 2d - 2q_f}{V_t^3 t_{prev}^3}, \tag{9}
$$

$$
b = \frac{-2V_t c t_{prev} + 3q_f - 3d}{V_t^2 t_{prev}^2}. \tag{10}
$$

The cubic spline curve has a different shape depending on t_{prev}, and t_{prev} is adapted in real time using the previous trajectory of the target vehicle. Equation(5) can be modified using (9) and (10) and discretized as follows:

$$
q_k = A_k \theta_k^3 + B_k \theta_k^2 + C_k \theta_k + D_k, \quad \theta_k = \frac{1}{t_{prev,k}}, \tag{11a}
$$

$$
A_k = \frac{2d - 2q_f}{V_t^3}(s_k - s_t)^3, \tag{11b}
$$

$$
B_k = \frac{c}{V_t^2}(s_k - s_t)^3 + \frac{3q_f - 3d}{V_t^2}(s_k - s_t)^2, \tag{11c}
$$

$$
C_k = -\frac{2c}{V_t}(s_k - s_t)^2, \tag{11d}
$$

$$
D_k = c(s_k - s_t) + d. \tag{11e}
$$

where θ_k denotes the reciprocal of preview time $t_{prev,k}$ and is an adaptation target parameter. V_t represents the longitudinal velocity measurement of the vehicle at the initial point of the path and is assumed to be constant while following the generated path. s_k and q_k denote the coordinates of the vehicle in the Frenet coordinate system.

Recursive least-squares estimation is a representative method for parameter adaptation [38]. This method applies least-squares estimation to the data accumulated in real time and is applicable only to linear models. The path used in this study is a cubic spline curve with nonlinearity. Therefore, t_{prev} adaptation is performed by applying LRLSE [39]. LRLSE operates in the same form as RLSE by calculating the slope of the function at every step, and uses nonlinear function values for residual calculation. t_{prev} is updated to minimize the sum of errors between the path and points passed by the target vehicle. The accuracy in estimating a time-invariant parameter can be increased when more trajectory data are accumulated. However, in the case of time-varying parameters, the more data are accumulated, the more difficult to respond to parameter changes. Therefore, by introducing a forgetting factor, the weights for the old and latest data are adjusted. The formulations of LRLSE are expressed as follows:

$$
f_k(\hat{\theta}_{k-1}) = A_k \hat{\theta}_{k-1}^3 + B_k \hat{\theta}_{k-1}^2 + C_k \hat{\theta}_{k-1} + D_k, \tag{12}
$$

$$
F_k(\hat{\theta}_{k-1}) = \left.\frac{\partial f_k(\theta)}{\partial \theta}\right|_{\theta = \hat{\theta}_{k-1}} = 3A_k \hat{\theta}_{k-1}^2 + 2B_k \hat{\theta}_{k-1} + C_k, \tag{13}
$$

$$
P_k = \frac{1}{\lambda}\left[P_{k-1} - \frac{P_{k-1} F_k F_k^T P_{k-1}}{\lambda + F_k^T P_{k-1} F_k}\right], \tag{14}
$$

$$
\hat{\theta}_k = \hat{\theta}_{k-1} + P_k F_k [q_{k,m} - f_k(\hat{\theta}_{k-1})], \tag{15}
$$

where $\hat{\theta}$, P, and λ are the unknown parameter, estimation-error covariance, and forgetting factor, respectively. $f_k(\hat{\theta}_{k-1})$

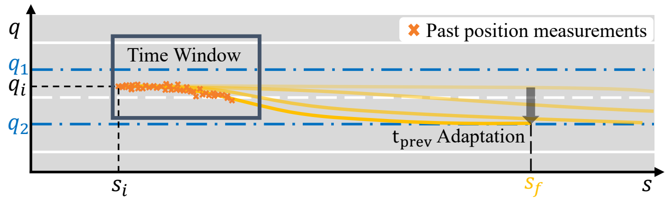

Fig. 3. Preview time adaptation process using LRLSE.

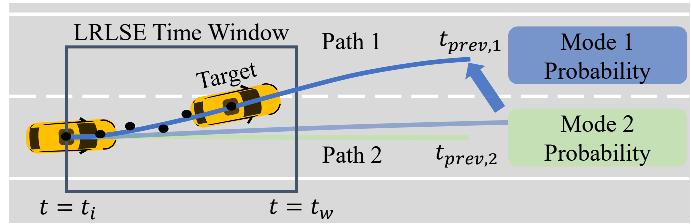

Fig. 4. Lane-change intention and future trajectory prediction.

is the q value calculated using the model (11a). $F_k(\hat{\theta}_{k-1})$ is the linearized form of $f_k(\hat{\theta}_{k-1})$ and used for P calculation. The parameter to be obtained through LRLSE is updated through innovation, which is the difference between the measured value $q_{k,m}$ and the calculated value $f_k(\hat{\theta}_{k-1})$ using the model. Moreover, λ is set within the range from 0 to 1, and the closer it is to 0, the lower the weight for older data.

Fig. 3 shows the process of adapting the preview time during the accumulation of the dataset. The scenario is that the target vehicle is driving in the upper lane and then changes lanes to the lower lane. The path is a cubic spline curve from the initial point (s_i, q_i) to the final point (s_f, q_2). q_2 is the distance between the center of the lower lane and the base frame. The final point of the path is determined by recursively updating t_{prev} by applying LRLSE to the points passed by the target vehicle within the time window. If the curvature of the past trajectory of the vehicle is small, then the intention to change lanes is weak and t_{prev} is large.

B. Multiple Model–Based Estimator (MME) Design for Lane Change–Intention Inference and Future Trajectory Prediction

In this subsection, we determine which path is most likely to be taken by a target vehicle out of multiple possible paths. To calculate the likelihood of the path, the measured and predicted values are compared using the model. The probability of each path is calculated using the likelihood, and the behavior of the target vehicle is predicted based on the path with the highest probability.

An MME is used to update the probabilities of each model and the state estimation result of the target vehicle while operating multiple path models in parallel [40]. There are two types of MMEs: static MME (SMME), which does not consider the transitions between models, and dynamic MME (DMME), which considers the transitions between models. In the DMME, the transition probability between models is determined using the transition probability matrix (TPM). If the TPM is reliable, the more versatile DMME performs better than the SMME in terms of accuracy and response time. The performance of the DMME is further enhanced if the TPM can be modified depending on the circumstance. In this study, models are updated in real time using past trajectories of the target vehicle. Model transition does not occur, but the model changes in real time depending on the situation. This simple form is similar to SMME and can show the effect of DMME where the TPM changes in real time. An MME with these characteristics is proposed as MMAE and applied to prediction of lane-change intention and future trajectory of the target vehicle.

As shown in Fig. 4, the target vehicle changes lanes to the left lane. When $t = t_i$, the paths from the location of the target vehicle to the center of the first lane and the center of the second lane are generated. For example, as shown in Fig. 4, the path is generated when the time is t_i and preview time adaptation is performed while the starting point of the path is fixed until the time is t_w. When the time is t_w, the path is re-generated from the location of the target vehicle and the same process is repeated. When regenerating the path, the preview time is the previous step estimate to minimize discontinuity. By adjusting the forgetting factor λ of LRLSE, responding to rapidly changing situations is possible by placing a large weight on recent trajectory data. The preview time of each path is adapted by applying LRLSE while accumulating the vehicle trajectory for the length of the time window. In the i^{th} LRLSE, estimation-error covariance $P_k[i]$ and innovation $r_k[i]$ are calculated. The likelihood $p(r_k[i]|m = i)$ of each path is calculated using $P_k[i]$ and $r_k[i]$. The likelihood is assumed to have a Gaussian distribution and is expressed as follows [41]:

$$p(r_k[i]|m = i) = \frac{exp\left(-r_k^T[i]P_k^{-1}[i]r_k[i]/2\right)}{(2\pi)^{n/2}|P_k[i]|^{1/2}}, \quad (16)$$

where $r_k[i]$ represents the difference between the measurement and model values in the i^{th} mode, $P_k[i]$ denotes the i^{th} mode estimation-error covariance, and n is the L0 norm of the measurement vector. As observed in (16), the smaller the estimation-error covariance and innovation, the higher the probability of the path. The mode probabilities for each path are calculated using the likelihood $p(r_k[i]|m = i)$, as shown in (17).

$$\alpha_k[i] = \frac{\alpha_{k-1}[i] \cdot p(r_k[i]|m = i)}{\sum_{j=1}^{M} \alpha_{k-1}[j] \cdot p(r_k[j]|m = j)}. \quad (17)$$

The i^{th} mode probability in the $(k-1)^{th}$ step and the likelihood in the k^{th} step are used to obtain the probability of the i^{th} mode in the k^{th} step. Particularly, the mode probability in the current step affects the mode probability in the next step. This is a form that reflects the lag effect that allows the mode probability to be updated gradually. M is the number of modes and indicates the number of lanes on the road. Fig. 5 presents the overall flow of the MMAE. For example, if three possible paths exist, then three LRLSEs are operated in parallel.

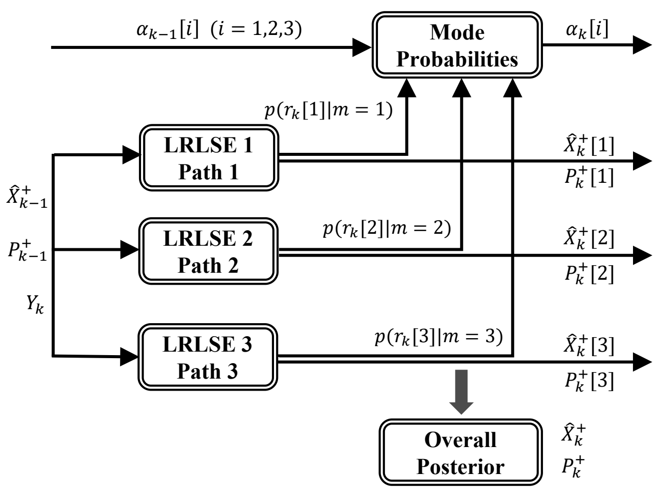

Fig. 5. Structure of the MMAE obtained using LRLSE.

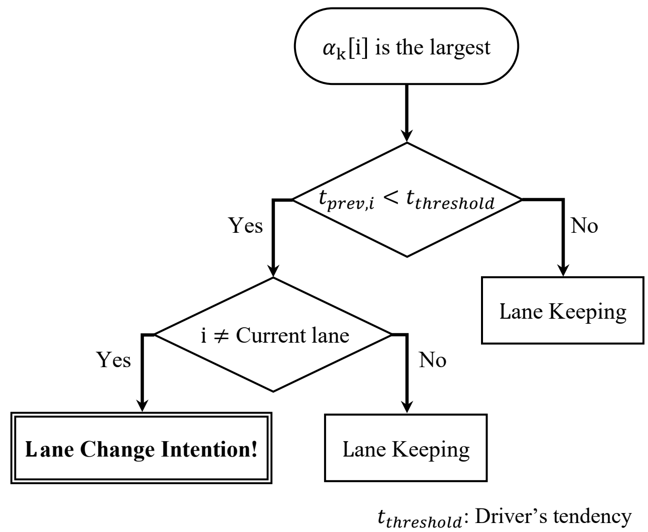

Fig. 6. Lane change–intention inference process using the MMAE.

The posterior $\hat{X}_{k-1}^+$ and the estimation-error covariance P_{k-1}^+ at the $(k-1)^{th}$ step are the inputs to each LRLSE. These values are arbitrarily set at the beginning of the algorithm operation. At each step, the likelihood is calculated for each mode by comparing the measured value and the value obtained using the model, and the mode probability is updated. For example, as shown in Fig. 4, when the target vehicle starts changing lanes, the preview time decreases so that path 1 matches the vehicle trajectory as much as possible and the mode probability α_1 for path 1 increases. Meanwhile, the difference between path 2 and the actual trajectory gradually increases so that the mode probability α_2 for path 2 decreases.

The mode probabilities and preview times of the MMAE are used to infer the lane-change intention of the target vehicle. The MMAE identifies the most probable path followed by the target vehicle using the mode probability for each path. Thereafter, lane-change intention is inferred using the preview time adaptation result of the path with the highest mode probability. Fig. 6 displays the flowchart of this process.

When the mode probability α_i of the i^{th} path is the highest, the lane-change intention is inferred using the preview time $t_{prev,i}$ for the i^{th} path adapted via LRLSE. When the final point of the i^{th} path with the highest mode probability does not belong to the currently driving lane area and $t_{prev,i}$ for this path is less than the threshold t_{th}, lane-change intention is observed. Conversely, if $t_{prev,i}$ is greater than t_{th} or if the final point of the i^{th} path is within the current driving lane, lane keeping is observed despite that α_i is the largest. The cubic spline curve for $t_{prev,i}$ that changes in real time is the result of predicting the future trajectory of the target vehicle for which lane-change intention is detected. For a rapid lane change with a large curvature of the accumulated trajectory, the length of the predicted future path is short because $t_{prev,i}$ is small.

IV. Test Results

This section verifies the performance of the MMAE in inferring lane-change intentions and predicting future trajectories using highD, which is a vehicle trajectory dataset on a German highway. Specifically, highD is a dataset that records the driving trajectories of real vehicles using a camera mounted on a drone in a specific section [42]. The latest computer vision technology was used to record traffic from six locations, and the length of each road is approximately 420 m. This dataset shows the type and size of the vehicle and contains information on the position, speed, and acceleration of each vehicle over time. Various situations, including lane change, are recorded, and the recorded typical positioning errors are less than 10 cm. The width of the lane is about 4 m, with the data sampling frequency of 25 Hz. In the highD dataset, the data of the vehicle changing lanes and the surrounding vehicles are collected, and the verification is performed on MATLAB.

Alternative approach for comparison with the proposed method: Look-ahead distance is a concept used in pure pursuit controllers for path tracking [43]. A bar with the same length of the look-ahead distance is attached to the center of the front of the target vehicle in the heading direction. If the bar crosses the right or left lane of the vehicle, an intention to change lanes in that direction is determined. As the highD dataset provides the global coordinates (x, y) of the upper-left corner of the bounding box of the vehicle, center coordinates (x_c, y_c) and bar-end coordinates (x_l, y_l) of the vehicle are obtained through coordinate transformation as follows:

$$(x_c, y_c) = \left(x - \frac{b}{2}sin\psi + \frac{a}{2}cos\psi, y + \frac{b}{2}cos\psi + \frac{a}{2}sin\psi\right), \tag{18}$$

$$(x_l, y_l) = (x_c + (l_d + a/2)cos\psi, y_c + (l_d + a/2)sin\psi), \tag{19}$$

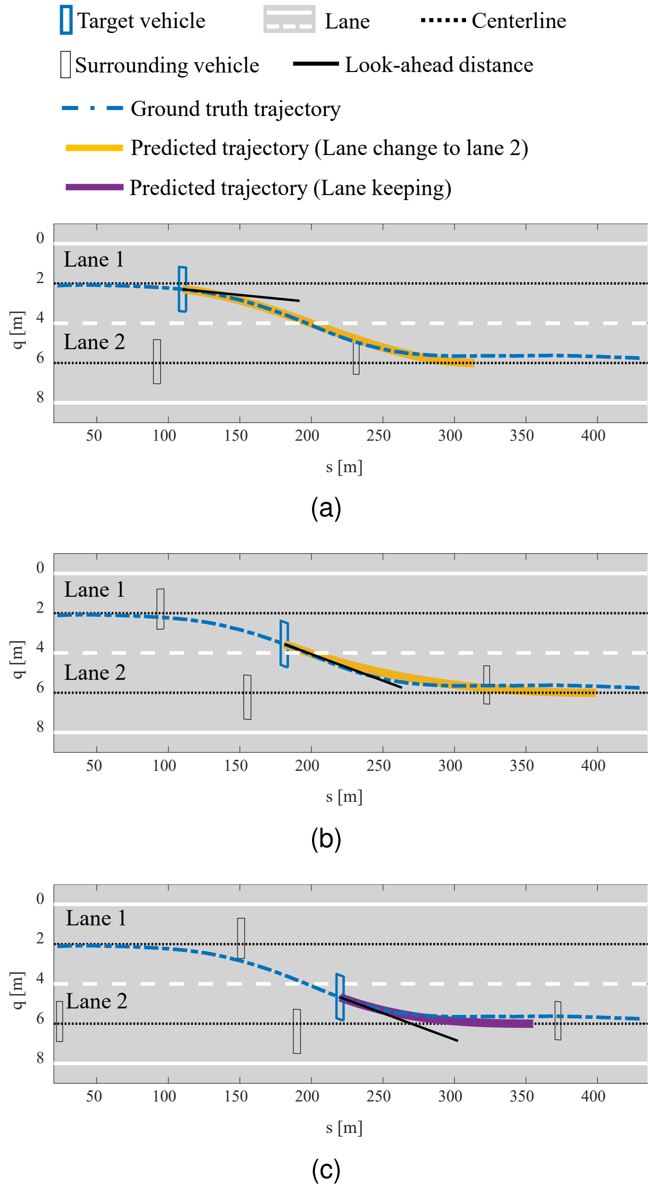

Fig. 7. Test results for Scenario 1: (a) lane-change initiation, (b) lane crossing, and (c) adjustment after lane change.

where ψ denotes the heading angle of the target vehicle, l_d represents the look-ahead distance, and a and b denote the length and width of the vehicle, respectively. If (x_l, y_l) is out of the current driving lane area, an intention to change the lane is determined and the coordinates of the lane are assumed to be known using the map. Further, l_d is $V_x * t_{look}$, and l_d is proportional to the longitudinal speed V_x of the vehicle. t_{look} has the similar concept as t_{prev} and is fixed at 3 s.

A. Scenario 1

1) Description and Analysis: As graphically shown in Fig. 7, the target vehicle changes lanes from lane 1 to lane 2 when all vehicles are driving to the right-hand side. White solid and white dashed lines represent lanes, and a black dotted line indicates the center of each lane. The blue and black boxes are the target vehicle and surrounding vehicles, respectively.

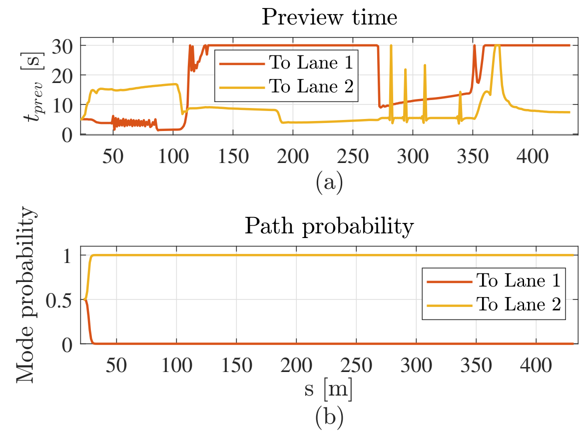

Fig. 8. Preview time and mode probability for each path in Scenario 1.

The size of the box is the same as that of the actual vehicle recorded in the highD dataset. As the length of the road is about 400 m, the longitudinal length of the box appears short. The blue dash–single dotted line represents the ground truth trajectory of the center of the target vehicle. Further, the yellow or purple solid line represents the future trajectory of the target vehicle predicted using the proposed MMAE. The solid black line denotes the look-ahead distance.

In Fig. 7(a), the target vehicle drives in the center of lane 1 and starts changing lanes toward lane 2. At this time, l_d is approximately 80 m, and as the end of the bar remains within lane 1, the look-ahead distance method cannot determine the intention to change lanes. However, the proposed method infers that the target vehicle will change lanes to the right through preview time and path probability for each path updated in real time and then predicts the future trajectory. The predicted future trajectory is similar to the actual trajectory of the target vehicle. In the lane change situation, the linear approximation error obtained by applying the LRLSE to the path with the highest mode probability is within 0.06 m and is calculated as follows [39]:

$$\varepsilon_k = f_k(\hat{\theta}_k) - F_k(\hat{\theta}_k)\left(\hat{\theta}_k - \hat{\theta}_{k-1}\right) - f_{k-1}(\hat{\theta}_{k-1}). \quad (20)$$

Fig. 7(b) shows the situation right before the center of the target vehicle crosses into lane 2. The predicted future trajectory remains the same as the actual one, but the error appears relatively large at the end of the trajectory. This is because of the assumption that the final point of the predicted future path is located at the center of the lane. Ideally, the vehicle drives along the centerline of the lane after changing lanes. However, in reality cases occur where the vehicle drives off-center. If an offset or overshoot occurs in a lane-change situation, then the future trajectory prediction result is different from the actual trajectory. Fig. 7(c) displays this tendency, which is a lane-keeping situation after changing lanes. Preview time adaptation is unnecessary in case of lane keeping; thus, the preview time is fixed at 5 s.

2) Preview Time Adaptation and Mode Probability: Fig. 8 presents the result of preview times and path probabilities for

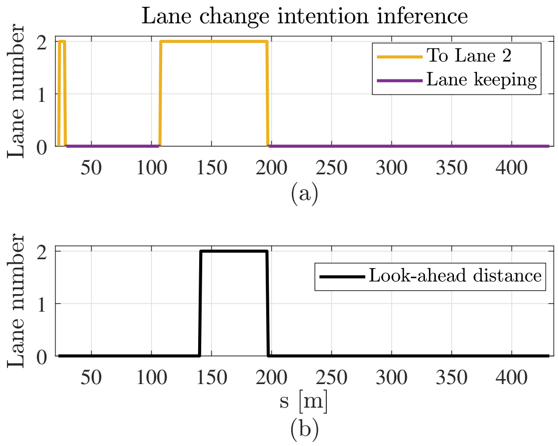

Fig. 9. Inference results of lane-change intention using the proposed MMAE and look-ahead distance method for Scenario 1.

TABLE I
LANE CHANGE–INTENTION INFERENCE PERFORMANCE OF THE LOOK-AHEAD DISTANCE METHOD ACCORDING TO t_{look} IN SCENARIO 1 ($\Delta t_{infer,MMAE} = 3.32s$)

$t_{look}(s)$	$\Delta t_{infer,look}(s)$	**inference result**
1	0.96	correct
2	1.64	correct
3	2.08	correct
4	2.4	correct
8	3.12	fail
10	3.4	fail

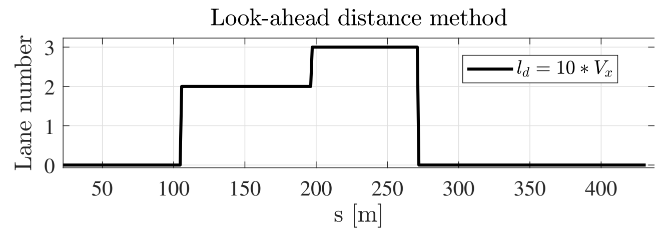

Fig. 10. Example of the look-ahead distance method incorrectly inferring the lane-change intention.

the paths to the center of each lane. In the algorithm of the MMAE, t_{th} is set to 10 s. If t_{prev} is greater than 10 s, then no intention to change lanes is determined regardless of path probability. Fig. 8(b) shows that the probability of the path to lane 2 is consistently 1. Fig. 8(a) shows that when s is 107 m, the preview time of the path to lane 2 is approximately 7 s. Hence, an intention to change lanes is inferred. When s is between 50 and 100 m, the target vehicle is in lane 1. In this section, the preview time $t_{prev,1}$ of the path from the target vehicle to the center of lane 1 tends to oscillate. When s is between 250 and 350 m, the target vehicle is in lane 2. Similarly, the preview time $t_{prev,2}$ of the path to the center of lane 2 is inconsistent. This problem can occur when a path close to a straight line is expressed as a cubic spline curve. As the path for lane keeping has an excessively small curvature, the stability of the curve fitting is reduced owing to the adaptation to a cubic spline curve. However, the preview time for the lane-keeping path is meaningless and only the preview time for the lane-change path is important. Therefore, the preview time of the lane-keeping path is used as a fixed value (i.e., 5 s). If the preview time becomes excessively large, it is considered irrelevant to the lane-change intention; hence, the upper limit is set to 30 s. If the logic presented in Fig. 6 is applied to the preview time and path probability results shown Fig. 8, the lane change–intention inference result presented in Fig. 9 can be obtained.

3) Lane Change Intention Inference: Fig. 9(a) presents the result when the proposed MMAE is applied to Scenario 1. Fig. 9(b) shows the result when the look-ahead distance method is used. In case of applying MMAE, the target vehicle is determined to temporarily follow the path toward lane 2 owing to the influence of the adaptation initial value before data are initially accumulated, but it immediately returns to lane keeping. Further, the MMAE infers the lane-change intention to lane 2 at the point where curvature occurs. Δt_{infer} denotes the time taken from the start of the lane change–intention inference until the center of the vehicle crosses the lane. If Δt_{infer} is large, there is enough time to plan a future path. $\Delta t_{infer,MMAE}$ obtained using the MMAE in this scenario is 3.32 s. When s exceeds 140 m, the look-ahead distance method infers the lane-change intention of the target vehicle and $\Delta t_{infer,look}$ is 2.08 s, which is 1.24 s later than the proposed method. Meanwhile, l_d is a variable for the longitudinal speed of the target vehicle, and t_{look} is set to 3 s by setting $l_d = 3 * V_x$. If t_{look} is increased, the look-ahead distance is also increased to ensure that the intention to change lanes can be quickly identified. However, if l_d is excessively long, then it is highly likely to erroneously infer that lane changes are made consecutively after the first lane change. Moreover, the sensitivity to the heading angle of the target vehicle increases due to the long l_d, and thus false alarms become frequent.

Table I presents the result of calculating $\Delta t_{infer,look}$ by applying the look-ahead distance method to the scenario presented in Fig. 7 with various t_{look}. If the look-ahead distance method infers that the vehicle maintains lane 2 after changing lanes from lane 1 to lane 2, then this prediction is "correct." If the method determines that the vehicle continuously changes lanes to lane 3, then this is represented as "fail" in the table. When t_{look} is set to a large value, $\Delta t_{infer,look}$ increases and failure does not occur until 4 s. However, when t_{look} is 5–10 s, failure occurs. To achieve similar performance as the MMAE ($\Delta t_{infer,MMAE} = 3.32s$), t_{look} must be set to greater than 9 s. Therefore, the proposed MMAE is better than the look-ahead distance method within the range of not making erroneous inferences(1–4 s).

Fig. 10 presents the result of the lane change–intention inference using the look-ahead distance method with $t_{look} = 10\,s$. The target vehicle is inferred to change lanes to lane 3 immediately after changing lanes to lane 2, but this is different from the actual behavior.

4) Trajectory Prediction: When the target vehicle changes lanes, the predicted future trajectory is compared with the actual trajectory to obtain the distance error distribution with

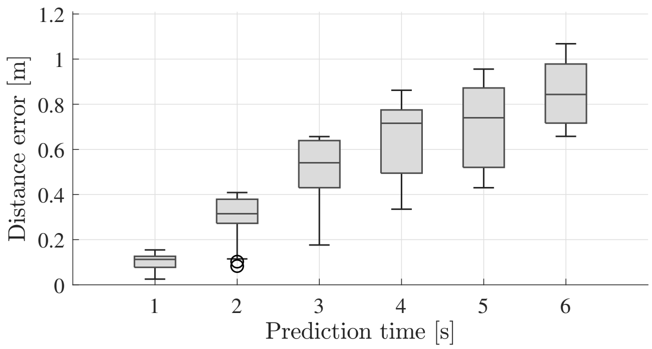

Fig. 11. Distance error distribution over the prediction time in Scenario 1.

respect to the prediction time (Fig. 11). The future trajectory is updated at every sampling time of 0.04 s, and 76 trajectories are included in this error distribution. The distance errors are listed in an ascending order for each prediction time. The 25% point of the data is the lower part of the box (lower quartile), the 75% point is the upper part of the box (upper quartile), and the 50% point is the line within the box (median). The interquartile range (IQR) denotes the size of the box. The whiskers connected to the boxes represent the maximum value within the range of up to 1.5 times the IQR upwards from the upper quartile and the minimum value within the range of up to 1.5 times the IQR downward from the lower quartile. The data outside the whiskers are circled as outliers. The future position is predicted by assuming that the longitudinal speed of the target vehicle is constant while passing through the predicted trajectory. In Fig. 11, the error when the prediction time is 4 s is between 0.3351 and 0.8621 m. The distance error is within 1 m until the prediction time is 5 s, and the maximum value of the error exceeds 1 m when the prediction time is 6 s. Because the target vehicle maintains a constant longitudinal speed of approximately 27 m/s while changing lanes, the predicted trajectory is quite similar to the real trajectory.

B. Scenario 2

1) Description and Analysis: Fig. 12 presents the second scenario. After the target vehicle changes lanes from lane 1 to lane 2, it drives in the direction of lane 1 again. The distance traveled while changing lanes in this scenario is shorter than that in previous scenarios. Fig. 12(a) shows the target vehicle starting to change lanes from lane 1 to lane 2. The MMAE infers the lane-change intention, but the look-ahead distance method cannot. The look-ahead distance l_d is approximately 82 m. The trajectory predicted by the MMAE immediately after the lane change–intention inference differs from the actual trajectory. Because the target vehicle rapidly changes lanes to lane 2, the curvature of the future trajectory is initially predicted to be small. As trajectory data with large curvature accumulates, the curvature becomes similar to that of the actual trajectory. Fig. 12(b) presents a lane-keeping situation, and if lane 3 exists, the look-ahead distance method infers that there is an intention to change lanes to lane 3. Fig. 12(c) shows the target vehicle starting to move toward lane 1 again. The MMAE infers that there is an intention to change

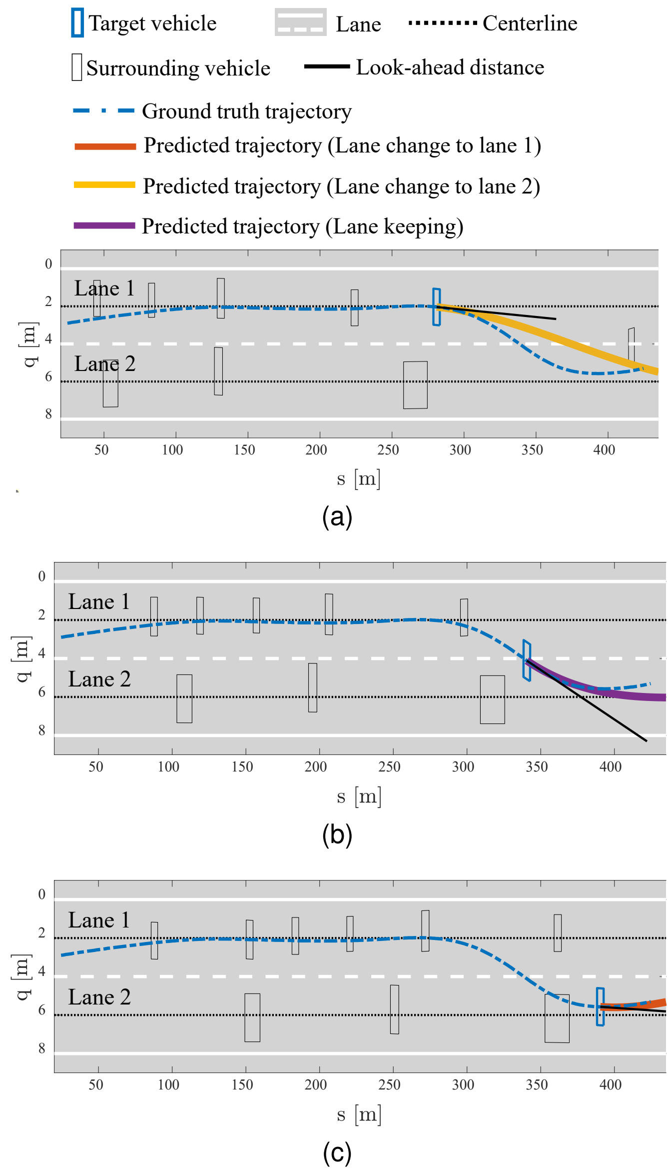

Fig. 12. Test results for Scenario 2. (a) Lane-change initiation, (b) lane crossing, and (c) lane-change initiation back to lane 1.

lanes to lane 1 and predicts the future trajectory similar to the actual trajectory. In the lane change situation, the linear approximation error obtained by applying the LRLSE to the path with the highest mode probability is within 0.2 m. If the curvature of the vehicle trajectory is large, the nonlinearity of the path increases. Therefore, the approximation error appears more significant than in the previous scenario. However, the order of error is mostly 10^{-2}, and even if it increases to 10^{-1}, it decreases again after a few steps.

2) Preview Time Adaptation and Mode Probability: As shown in Fig. 13(b), the target vehicle drives in lane 1 in the range of s from 100 to 300 m but the probability of the path toward lane 2 is high. However, as shown in Fig. 13(a), the preview time for the same section is greater than $t_{th} = 10s$. Therefore, the target vehicle maintains the lane. The characteristic of the cubic spline curve, where the probability of a path of lane change is higher than that of a

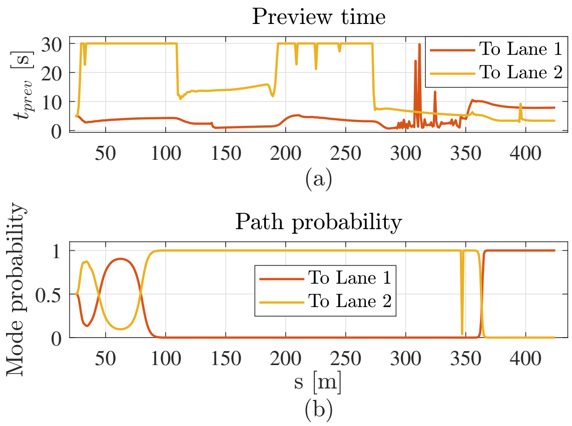

Fig. 13. Preview time and mode probability for each path in Scenario 2.

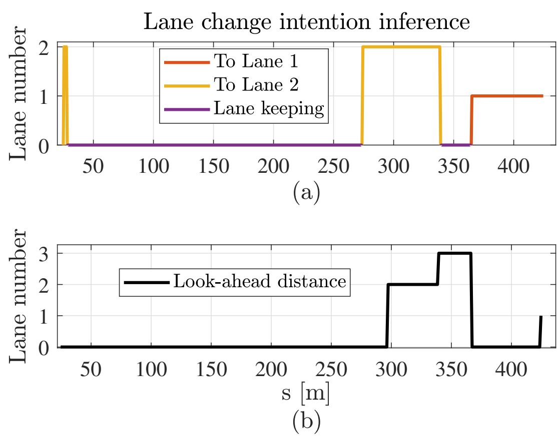

Fig. 14. Inference results of lane-change intention using the proposed MMAE and look-ahead distance method for Scenario 2.

TABLE II
LANE CHANGE–INTENTION INFERENCE PERFORMANCE OF THE LOOK-AHEAD DISTANCE METHOD ACCORDING TO t_{look} IN SCENARIO 2 ($\Delta t_{infer,MMAE} = 2.4s$)

$t_{look}(s)$	$\Delta t_{infer,look}(s)$	**inference result**
1	0.88	correct
2	1.32	correct
3	1.56	fail
10	2.16	fail
20	2.4	fail

path of lane keeping, allows quick recognition of the intention to change lanes. That is, the MMAE watches the lane-change path more closely. As shown in Fig. 13(a), when s is 300 m, the preview time for the lane-keeping path appears unstable. The preview time for the lane-keeping path uses a fixed value (5 s); thus, the unstable t_{prev} is not used. However, the probability of the path toward lane 1 increases when s is 360 m. As the preview time to lane 1 is within 10 s, an intention to change lanes to lane 1 again is inferred. Fig. 14 presents the results of lane change–intention inference.

3) Lane Change Intention Inference: Figs. 14(a) and 14(b) present the results of the MMAE and look-ahead distance method, respectively. $\Delta t_{infer,MMAE} = 2.4s$ is 0.84 s faster than $\Delta t_{infer,look} = 1.56s$. In addition, the look-ahead distance method incorrectly infers the lane-change intention to lane 3 and infers the intention to change lanes again to lane 1 very late.

Table II presents the performance of the look-ahead distance method according to t_{look}. The maximum value of $\Delta t_{infer,look}$ in the correct range is 1.32 s, half of $\Delta t_{infer,MMAE}$. To make $\Delta t_{infer,look}$ equal to $\Delta t_{infer,MMAE}$, t_{look} must be increased up to 20 s. In this case, l_d is approximately 546 m. Therefore, the look-ahead distance method is vulnerable to rapid lane changes similar to this scenario. It can be concluded that the MMAE exhibits advantages with respect to inference speed and robustness.

4) Trajectory Prediction: Fig. 15 shows the distance error distribution for the prediction time by comparing 60 future trajectories predicted in a lane-change situation with the actual trajectory. The length of the predicted trajectory is short because the lane change is made abruptly. Hence, the prediction time appears to be up to 3 s and the distance error for future time is less than 2 m. Because the curvature of the lane-change trajectory is large, the maximum error in the lateral direction of the initially predicted trajectory is close to 2 m. However, the lateral error decreases as trajectories with large curvature data accumulate.

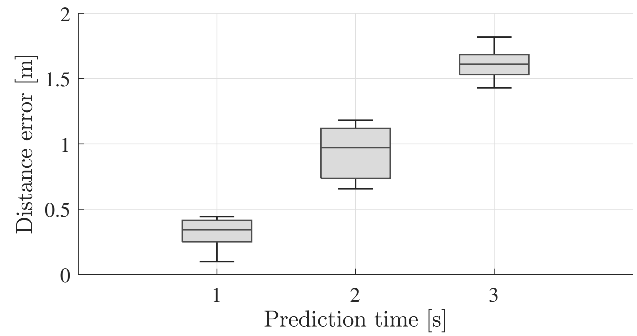

Fig. 15. Distance error distribution over the prediction time in Scenario 2.

C. Verification of MMAE Performance in Various Scenarios

1) Lane Change Intention Inference: Table III presents the result of calculating $\Delta t_{infer,MMAE}$ by applying the MMAE to various scenarios and by comparing it with $\Delta t_{infer,look}$. The ID of the target vehicle is the number recorded in the highD dataset. The results of applying the MMAE afford two cases when t_{th} is 10 s and 15 s each. t_{th} is a tuning parameter that can be adjusted according to the driver's tendency regarding the lane-change detection. If t_{th} is large, the lane-change intention can be quickly identified even when the lane-change curvature is small. However, if t_{th} is set too high, a false alarm may be generated in response to even a slight curvature. Most of the lane-change time is within 15 s, and even if in some cases it exceed 15 s, this is not threatening; hence, t_{th} is set to 15 s or less.

Fig. 16 shows Table III as a bar chart. In all cases, the MMAE with t_{th} of 15 s shows better performance than the

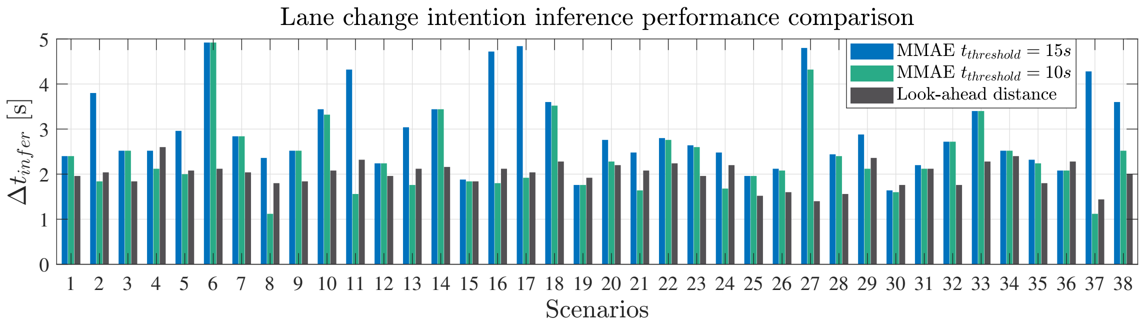

Fig. 16. Bar chart comparing lane change–intention inference performance of the MMAE and look-ahead distance method for various scenarios.

TABLE III
LANE CHANGE–INTENTION INFERENCE PERFORMANCE COMPARISON OF THE MMAE AND LOOK-AHEAD DISTANCE METHOD FOR VARIOUS SCENARIOS

ID	$\Delta t_{infer,MMAE}(s)$ $(t_{th} = 15s)$	$\Delta t_{infer,MMAE}(s)$ $(t_{th} = 10s)$	$\Delta t_{infer,look}(s)$ $(t_{look} = 3s)$
60	2.4	2.4	1.96
97	3.8	1.84	2.04
111	2.52	2.52	1.84
115	2.52	2.12	2.6
118	2.96	2	2.08
137	4.92	4.92	2.12
172	2.84	2.84	2.04
188	2.36	1.12	1.8(fail)
213	2.52	2.52	1.84
228	3.44	3.32	2.08
237	4.32	1.56	2.32
274	2.24	2.24	1.96
326	3.04	1.76	2.12
391	3.44	3.44	2.16
395	1.88	1.84	1.84
447	4.72	1.8	2.12
455	4.84	1.92	2.04
535	3.6	3.52	2.28
550	1.76	1.76	1.92
555	2.76	2.28	2.2
565	2.48	1.64	2.08
641	2.8	2.76	2.24
646	2.64	2.6	1.96
654	2.48	1.68	2.2
677	1.96	1.96	1.52
728	2.12	2.08	1.6(fail)
730	4.8	4.32	1.4
739	2.44	2.4	1.56(fail)
778	2.88	2.12	2.36
789	1.64	1.6	1.76
803	2.2	2.12	2.12
851	2.72	2.72	1.76(fail)
858	3.4	3.4	2.28
865	2.52	2.52	2.4
873	2.32	2.24	1.8
920	2.08	2.08	2.28
929	4.28	1.12	1.44
966	3.6	2.52	2
Mean	2.68	2.18	2.04

MMAE with t_{th} of 10 s. The cases where t_{th} is different but $\Delta t_{infer,MMAE}$ is the same represent lane change from the beginning of the scenario. When the target vehicle changes lanes using a trajectory with a small curvature, the performance determined according to t_{th} tends to be considerably different than usual. In most cases $\Delta t_{infer,MMAE}$ is greater than $\Delta t_{infer,look}$. However, in Case 8, for example, the performance of the $t_{th} = 10s$ MMAE is lower than that of the look-ahead distance method. In some cases (e.g., Case 30), the performance of the look-ahead distance method is the best. However, the look-ahead distance method sometimes produces inference results different from the reality and $\Delta t_{infer,MMAE}$ of the MMAE is high on average. In particular, many cases exist where the performance of the MMAE with the t_{th} of 15 s is considerably better than that of the look-ahead distance method.

TABLE IV
COMPARISON OF THE LANE CHANGE-INTENTION INFERENCE PERFORMANCE OF EXISTING METHODS AND MMAE

Approach	**Accuracy** (%)	$\Delta t_{infer}(s)$
ANN [15]	98.3	2.33
Back-propagation NN [20]	85.4	1.5
HMM [13]	87.4	7.08
MMAE $(t_{th} = 15s)$	-	**2.68**
SVM (Benterki *et al.*) [15]	95.7	1.95
SVM (Woo *et al.*) [14]	98.1	1.74

Table IV compares the lane change-intention inference performance of MMAE with previous studies. The proposed method infers lane-change intention before the target vehicle crosses the lane if the reliability of position and speed measurements is guaranteed. Therefore, MMAE focuses on Δt_{infer} rather than accuracy, and accuracy is indicated for comparison between existing ML-based methods. ANN has the highest accuracy, while Δt_{infer} is also relatively long. HMM exhibits an overwhelmingly long Δt_{infer}, but is somewhat less accurate. MMAE has longer Δt_{infer} compared to methods using SVM and back-propagation NN, and is at a similar level to ANN. Therefore, the proposed method has sufficient competitiveness compared to ML-based methods.

2) Trajectory Prediction: Fig. 17 presents the distance error mean distribution based on the prediction time in various scenarios. The target vehicles are identical to the IDs presented in Table III, except for IDs 115, 237, 326, 565, and 654, where it is difficult to compare the predicted future trajectories with the actual trajectories or the prediction time is less than 3 s. This plot shows the average distance error based on the prediction time for each vehicle ID, and the prediction time

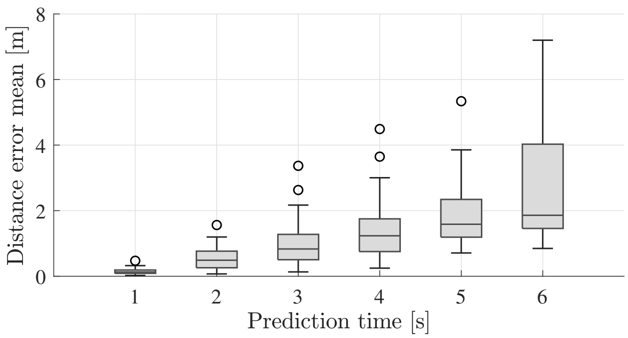

Fig. 17. Distance error mean distribution over the prediction time in various scenarios.

TABLE V
TRAJECTORY PREDICTION RMSE OF EXISTING STUDIES IN METERS OVER PREDICTION TIME

Approach	Prediction time (s) 1	2	3	4	5
CNN-LSTM [30]	0.64	0.96	1.22	1.53	2.09
CS-LSTM [24]	0.22	0.61	1.24	2.10	3.27
GP [23]	1.58	2.68	3.37	-	-
L-RRNN [44]	0.22	0.65	1.31	2.22	3.38
MATF GAN [45]	0.66	1.34	2.08	2.97	4.13
MHA-LSTM [24]	0.19	0.55	1.10	1.84	2.78
MHA-LSTM(+f) [24]	**0.06**	**0.09**	**0.24**	**0.59**	**1.18**
NLS-LSTM [24]	0.20	0.57	1.14	1.90	2.91
S-LSTM [24]	0.22	0.62	1.27	2.15	3.41
Sc-LSTM [44]	0.32	0.82	1.60	2.63	3.87
Sc-RRNN [44]	0.29	0.69	1.33	2.22	3.33
V-LSTM [44]	0.31	0.81	1.51	2.48	3.71

varies according to the length of the predicted trajectory. For example, as shown in Fig. 15, if the average distance error is obtained for each prediction time, it is 0.3248, 0.9369, and 1.6161 m in this order. For the remaining 32 scenarios, the average distance errors are calculated and a box plot is drawn. The variance of the average of the distance errors for each prediction time tends to become larger, but the median is within 2 m at 6 s. The points on the outlier indicate a scenario where the curvature of the trajectory rapidly changes. Even in this case, the distance error can be reduced while accumulating the trajectory data. Therefore, the future trajectory predicted by reflecting the past trajectory of the target vehicle in real time using the MMAE is similar to the actual trajectory.

Table V shows the trajectory prediction performance of ML-based existing studies. Researches based on LSTM have been actively conducted, and the performance of MHA-LSTM (+f) is particularly overwhelming. Therefore, we compare the proposed method with MHA-LSTM (+f) and verify its effectiveness.

Table VI presents the trajectory prediction performance of the proposed MMAE when compared with those of other approaches. The IMM-based method uses a physics model and a maneuver model, and the model with the largest mode probability determines the behavior of the target vehicle. The

TABLE VI
COMPARISON OF THE TRAJECTORY PREDICTION RESULTS CONCERNING THE MEAN ABSOLUTE ERROR IN METERS OVER PREDICTION TIME

Approach	Prediction time (s) 1	3	5
Physics-based [25]	0.193	1.478	3.493
IMM-based [25]	0.150	1.315	2.931
MHA-LSTM (+f) [24]	0.202	0.461	1.907
MMAE (Proposed)	**0.154**	**1.047**	**2.046**

result of the MHA-LSTM (+f) method is the mean absolute error (MAE) calculated only for a lane-change situation. The MAE is considered the average distance error between the actual and predicted positions for each prediction time as follows:

$$MAE = \frac{1}{N}\sum_{i=1}^{N}\sqrt{(s_{real,i} - s_{pred,i})^2 + (q_{real,i} - q_{pred,i})^2}. \tag{21}$$

The results of the physics- and IMM-based methods were applied to the driving data of the experimental vehicle, and those of the MHA-LSTM (+f) and MMAE methods were verified using the highD dataset. The proposed method was found to be more accurate than the physics- and IMM-based methods. MMAE tends to have a slightly larger error than MHA-LSTM (+f), which recorded the highest accuracy among ML-based methods. However, when the prediction time is 5 s, the MAEs of both MMAE and MHA-LSTM (+f) are similar to about 2 m. The MMAE does not require big data for training and can predict trajectories with a low computation burden. Therefore, the proposed algorithm exhibits advantages in prediction performance and can successfully perform lane change–intention inference and trajectory prediction simultaneously.

V. CONCLUSION

This paper proposed an MMAE that simultaneously performs multiple LRLSEs to infer the lane-change intention of the surrounding vehicles and to predict the lane-change trajectory on the highway. Initially, a path was generated as a cubic spline curve in the Frenet coordinate system. The final point of the path was determined based on the longitudinal speed and preview time of the target vehicle. Preview time adaptation was performed through LRLSE, which can consider the nonlinearity of the model. The MMAE can calculate each mode probability of the paths.

The proposed method is evaluated using the highD dataset. The MMAE infers the target vehicle's lane-change intention and is more robust than other methods. Based on the comparison of the predicted and actual trajectories in various scenarios, the median of the average distance error after 6 s is less than 2 m. The MMAE shows excellent performance without using a massive amount of training data, and the algorithm exhibits high real-time performance and a low computational burden.

In the future, we will plan a path that minimizes the risk of ego AVs based on the results of the lane change–intention inference and future trajectory prediction of the surrounding vehicles. We will finally proceed to path-tracking control to improve the CAS reliability.

REFERENCES

[1] J. Nidamanuri, C. Nibhanupudi, R. Assfalg, and H. Venkataraman, “A progressive review-emerging technologies for adas driven solutions,” *IEEE Transactions on Intelligent Vehicles*, 2021.

[2] J. Dahl, G. R. de Campos, C. Olsson, and J. Fredriksson, “Collision avoidance: A literature review on threat-assessment techniques,” *IEEE Transactions on Intelligent Vehicles*, vol. 4, no. 1, pp. 101–113, 2018.

[3] M. Shawky, “Factors affecting lane change crashes,” *IATSS research*, vol. 44, no. 2, pp. 155–161, 2020.

[4] A. Alizadeh, M. Moghadam, Y. Bicer, N. K. Ure, U. Yavas, and C. Kurtulus, “Automated lane change decision making using deep reinforcement learning in dynamic and uncertain highway environment,” in *2019 IEEE intelligent transportation systems conference (ITSC)*. IEEE, 2019, pp. 1399–1404.

[5] J. Wang, Q. Zhang, D. Zhao, and Y. Chen, “Lane change decision-making through deep reinforcement learning with rule-based constraints,” in *2019 International Joint Conference on Neural Networks (IJCNN)*. IEEE, 2019, pp. 1–6.

[6] P. Hang, C. Lv, Y. Xing, C. Huang, and Z. Hu, “Human-like decision making for autonomous driving: A noncooperative game theoretic approach,” *IEEE Transactions on Intelligent Transportation Systems*, vol. 22, no. 4, pp. 2076–2087, 2020.

[7] V. G. Lopez, F. L. Lewis, M. Liu, Y. Wan, S. Nageshrao, and D. Filev, “Game-theoretic lane-changing decision making and payoff learning for autonomous vehicles,” *IEEE Transactions on Vehicular Technology*, vol. 71, no. 4, pp. 3609–3620, 2022.

[8] Y. Liu, X. Wang, L. Li, S. Cheng, and Z. Chen, “A novel lane change decision-making model of autonomous vehicle based on support vector machine,” *IEEE access*, vol. 7, pp. 26 543–26 550, 2019.

[9] A. Mechernene, V. Judalet, A. Chaibet, and M. Boukhnifer, “Lane change decision algorithm based on risk prediction and fuzzy logic method,” in *2021 25th International Conference on System Theory, Control and Computing (ICSTCC)*. IEEE, 2021, pp. 707–713.

[10] K. Ji, N. Li, M. Orsag, and K. Han, “Hierarchical and game-theoretic decision-making for connected and automated vehicles in overtaking scenarios,” *Transportation Research Part C: Emerging Technologies*, vol. 150, p. 104109, 2023.

[11] A. Abraham, Y. Zhang, and S. Prasad, “Real-time prediction of multi-class lane-changing intentions based on highway vehicle trajectories,” in *2021 IEEE International Intelligent Transportation Systems Conference (ITSC)*. IEEE, 2021, pp. 1457–1462.

[12] T. Han, J. Jing, and Ü. Özgüner, “Driving intention recognition and lane change prediction on the highway,” in *2019 IEEE Intelligent Vehicles Symposium (IV)*. IEEE, 2019, pp. 957–962.

[13] Y. Xia, Z. Qu, Z. Sun, and Z. Li, “A human-like model to understand surrounding vehicles’ lane changing intentions for autonomous driving,” *IEEE Transactions on Vehicular Technology*, vol. 70, no. 5, pp. 4178–4189, 2021.

[14] H. Woo, Y. Ji, H. Kono, Y. Tamura, Y. Kuroda, T. Sugano, Y. Yamamoto, A. Yamashita, and H. Asama, “Lane-change detection based on vehicle-trajectory prediction,” *IEEE Robotics and Automation Letters*, vol. 2, no. 2, pp. 1109–1116, 2017.

[15] A. Benterki, M. Boukhnifer, V. Judalet, and M. Choubeila, “Prediction of surrounding vehicles lane change intention using machine learning,” in *2019 10th IEEE International Conference on Intelligent Data Acquisition and Advanced Computing Systems: Technology and Applications (IDAACS)*, vol. 2. IEEE, 2019, pp. 839–843.

[16] X. Li, W. Wang, and M. Roetting, “Estimating driver’s lane-change intent considering driving style and contextual traffic,” *IEEE Transactions on Intelligent Transportation Systems*, vol. 20, no. 9, pp. 3258–3271, 2018.

[17] J. Tang, S. Yu, F. Liu, X. Chen, and H. Huang, “A hierarchical prediction model for lane-changes based on combination of fuzzy c-means and adaptive neural network,” *Expert systems with applications*, vol. 130, pp. 265–275, 2019.

[18] W. Wang, T. Qie, C. Yang, W. Liu, C. Xiang, and K. Huang, “An intelligent lane-changing behavior prediction and decision-making strategy for an autonomous vehicle,” *IEEE Transactions on Industrial Electronics*, vol. 69, no. 3, pp. 2927–2937, 2021.

[19] B. Morris, A. Doshi, and M. Trivedi, “Lane change intent prediction for driver assistance: On-road design and evaluation,” in *2011 IEEE Intelligent Vehicles Symposium (IV)*. IEEE, 2011, pp. 895–901.

[20] J. Peng, Y. Guo, R. Fu, W. Yuan, and C. Wang, “Multi-parameter prediction of drivers’ lane-changing behaviour with neural network model,” *Applied ergonomics*, vol. 50, pp. 207–217, 2015.

[21] G. Xie, H. Gao, L. Qian, B. Huang, K. Li, and J. Wang, “Vehicle trajectory prediction by integrating physics-and maneuver-based approaches using interactive multiple models,” *IEEE Transactions on Industrial Electronics*, vol. 65, no. 7, pp. 5999–6008, 2017.

[22] C. Wissing, T. Nattermann, K.-H. Glander, and T. Bertram, “Trajectory prediction for safety critical maneuvers in automated highway driving,” in *2018 21st International Conference on Intelligent Transportation Systems (ITSC)*. IEEE, 2018, pp. 131–136.

[23] Y. Yoon, C. Kim, J. Lee, and K. Yi, “Interaction-aware probabilistic trajectory prediction of cut-in vehicles using gaussian process for proactive control of autonomous vehicles,” *IEEE Access*, vol. 9, pp. 63 440–63 455, 2021.

[24] K. Messaoud, I. Yahiaoui, A. Verroust-Blondet, and F. Nashashibi, “Attention based vehicle trajectory prediction,” *IEEE Transactions on Intelligent Vehicles*, vol. 6, no. 1, pp. 175–185, 2020.

[25] X. Liu, Y. Wang, Z. Zhou, K. Nam, C. Wei, and C. Yin, “Trajectory prediction of preceding target vehicles based on lane crossing and final points generation model considering driving styles,” *IEEE Transactions on Vehicular Technology*, vol. 70, no. 9, pp. 8720–8730, 2021.

[26] X. Tang, K. Yang, H. Wang, J. Wu, Y. Qin, W. Yu, and D. Cao, “Prediction-uncertainty-aware decision-making for autonomous vehicles,” *IEEE Transactions on Intelligent Vehicles*, 2022.

[27] N. Lyu, J. Wen, Z. Duan, and C. Wu, “Vehicle trajectory prediction and cut-in collision warning model in a connected vehicle environment,” *IEEE Transactions on Intelligent Transportation Systems*, vol. 23, no. 2, pp. 966–981, 2020.

[28] Y.-Y. Ren, L. Zhao, X.-L. Zheng, and X.-S. Li, “A method for predicting diverse lane-changing trajectories of surrounding vehicles based on early detection of lane change,” *IEEE Access*, vol. 10, pp. 17 451–17 472, 2022.

[29] N. Deo and M. M. Trivedi, “Multi-modal trajectory prediction of surrounding vehicles with maneuver based lstms,” in *2018 IEEE Intelligent Vehicles Symposium (IV)*. IEEE, 2018, pp. 1179–1184.

[30] X. Mo, Y. Xing, and C. Lv, “Interaction-aware trajectory prediction of connected vehicles using cnn-lstm networks,” in *IECON 2020 The 46th Annual Conference of the IEEE Industrial Electronics Society*. IEEE, 2020, pp. 5057–5062.

[31] L. Xiong, Z. Fu, D. Zeng, and B. Leng, “Surrounding vehicle trajectory prediction and dynamic speed planning for autonomous vehicle in cut-in scenarios,” in *2021 IEEE Intelligent Vehicles Symposium (IV)*. IEEE, 2021, pp. 987–993.

[32] Y. Huang, J. Du, Z. Yang, Z. Zhou, L. Zhang, and H. Chen, “A survey on trajectory-prediction methods for autonomous driving,” *IEEE Transactions on Intelligent Vehicles*, 2022.

[33] J. Dahl, G. R. de Campos, and J. Fredriksson, “Performance and efficiency analysis of a linear learning-based prediction model used for unintended lane-departure detection,” *IEEE Transactions on Intelligent Transportation Systems*, vol. 23, no. 7, pp. 9115–9125, 2021.

[34] K. Chu, M. Lee, and M. Sunwoo, “Local path planning for off-road autonomous driving with avoidance of static obstacles,” *IEEE transactions on intelligent transportation systems*, vol. 13, no. 4, pp. 1599–1616, 2012.

[35] J. Hayakawa and B. Dariush, “Ego-motion and surrounding vehicle state estimation using a monocular camera,” in *2019 IEEE Intelligent Vehicles Symposium (IV)*. IEEE, 2019, pp. 2550–2556.

[36] D. D. Yoon, B. Ayalew, and G. M. N. Ali, “Performance of decentralized cooperative perception in v2v connected traffic,” *IEEE Transactions on Intelligent Transportation Systems*, vol. 23, no. 7, pp. 6850–6863, 2021.

[37] H. Wang, J. Kearney, and K. Atkinson, “Robust and efficient computation of the closest point on a spline curve,” in *Proceedings of the 5th International Conference on Curves and Surfaces*, 2002, pp. 397–406.

[38] T. Lee, D.-H. Kim, and S. B. Choi, “Driveline modeling with transmission loss and robust torque observer design for dual clutch transmission,” *IEEE Transactions on Vehicular Technology*, vol. 71, no. 2, pp. 1267–1279, 2021.

[39] M. Choi, J. J. Oh, and S. B. Choi, “Linearized recursive least squares methods for real-time identification of tire–road friction coefficient,” *IEEE Transactions on Vehicular Technology*, vol. 62, no. 7, pp. 2906–2918, 2013.

[40] Y. Bar-Shalom, X. R. Li, and T. Kirubarajan, *Estimation with applications to tracking and navigation: theory algorithms and software*. John Wiley & Sons, 2004.
[41] D. Simon, *Optimal state estimation: Kalman, H infinity, and nonlinear approaches*. John Wiley & Sons, 2006.
[42] R. Krajewski, J. Bock, L. Kloeker, and L. Eckstein, "The highd dataset: A drone dataset of naturalistic vehicle trajectories on german highways for validation of highly automated driving systems," in *2018 21st International Conference on Intelligent Transportation Systems (ITSC)*. IEEE, 2018, pp. 2118–2125.
[43] J. Liu, Z. Yang, Z. Huang, W. Li, S. Dang, and H. Li, "Simulation performance evaluation of pure pursuit, stanley, lqr, mpc controller for autonomous vehicles," in *2021 IEEE International Conference on Real-time Computing and Robotics (RCAR)*. IEEE, 2021, pp. 1444–1449.
[44] K. Messaoud, I. Yahiaoui, A. Verroust-Blondet, and F. Nashashibi, "Relational recurrent neural networks for vehicle trajectory prediction," in *2019 IEEE Intelligent Transportation Systems Conference (ITSC)*. IEEE, 2019, pp. 1813–1818.
[45] T. Zhao, Y. Xu, M. Monfort, W. Choi, C. Baker, Y. Zhao, Y. Wang, and Y. N. Wu, "Multi-agent tensor fusion for contextual trajectory prediction," in *Proceedings of the IEEE/CVF Conference on Computer Vision and Pattern Recognition*, 2019, pp. 12 126–12 134.

Jongyong Do received his B.S. and M.S. degrees in mechanical engineering from Korea Advanced Institute of Science and Technology (KAIST), Daejeon, South Korea. He is currently working toward his Ph.D. degree at KAIST. His research interests include vehicle dynamics, control theory, vehicle-motion prediction, and active safety systems.

Kyoungseok Han received his B.S. degree in civil engineering (minor in mechanical engineering) from Hanyang University, Seoul, South Korea, in 2013 and his M.S. and Ph.D. degrees in mechanical engineering from KAIST, Daejeon, South Korea, in 2015 and 2018, respectively. He was a Research Fellow at the University of Michigan from June 2018 to February 2020. In March 2020, he was appointed as an Assistant Professor at the School of Mechanical Engineering, Kyungpook National University. His current research interests include vehicle dynamics and control, autonomous vehicle, battery electric vehicle, optimization, and control theory.

Seibum B. Choi (M'09) received his B.S. in mechanical engineering from Seoul National University, Seoul, South Korea, M.S. in mechanical engineering from KAIST, Daejeon, South Korea, and Ph.D. in control from the University of California, Berkeley, CA, USA, in 1993. From 1993 to 1997, he was involved in the development of automated vehicle–control systems at the Institute of Transportation Studies, University of California. Through 2006, he was with TRW, Livonia, MI, USA, where he was involved in the development of advanced vehicle control systems. Since 2006, he has been a member of the faculty of the Mechanical Engineering Department, KAIST, South Korea. His current research interests include fuel-saving technology, vehicle dynamics and control, and active safety systems. Prof. Choi is a Member of the American Society of Mechanical Engineers, Society of Automotive Engineers, and Korean Society of Automotive Engineers.